THE JOURNAL OF PHYSICAL CHEMISTRY C

Article

pubs.acs.org/JPCC

Reversible Anion Exchange Reaction in Solid Halide Perovskites and Its Implication in Photovoltaics

Guijun Li,* Jacob Yuek-Lung Ho, Man Wong, and Hoi Sing Kwok*

State Key Lab on Advanced Displays and Optoelectronics Technologies, Department of Electronic and Computer Engineering, Hong Kong University of Science and Technology, Clear Water Bay, Kowloon, Hong Kong

Supporting Information

ABSTRACT: Anion exchange reaction is a particularly versatile tool for the synthesis of a large class of nanomaterials. Here we report a low temperature, fast, reversible anion exchange reaction in halide perovskite thin film. Although processed in the solid-state phase, the exchanged hybrid perovskite shows good quality in terms of morphology conservation, phase transformation, and homogeneous composition. The easily exchanged reaction during the crystallization process suggests the robust nature of the Pb−CH_3NH_3 framework and high diffusion ability of halide ions in the perovskite lattice. Furthermore, we show its application in perovskite solar cells; we find that the anion exchange reaction does not induce any remarkable defects resulting from the lattice transformation and morphology reconstruction. In some case, the beneficial exchange of halide species involving simultaneous displacement reaction and crystallization can be used to improve the perovskite solar cell performance. Our work provides new physical insight into understanding the perovskite formation mechanism and the ionic behavior in the perovskite.

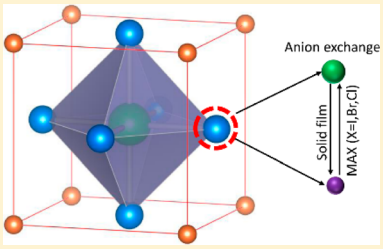

1. INTRODUCTION

Over the past few years, metal halide perovskites have attracted tremendous interest due to their unique and promising properties.[1−5] The high power conversion efficiency of the perovskite solar cell larger than 20% makes them comparable to the other leading thin-film solar cells,[1] such as those using Cu(In,Ga)Se_2 or CdTe. Despite the rapid progress in perovskite solar cells, there remains a considerable gap in our fundamental understanding of the perovskite formation mechanism and physical/chemical reactivity.

Currently, the fabrication process has usually relied on the direct reaction of two precursors in the solution phase, followed by low temperature annealing subsequently employed to facilitate solvent evaporation and crystallization.[6] Up to this point, postsynthetic transformation methods, such as ion exchange reactions, have not received much attention from the scientific community for the fabrication of halide perovskites, although they have been proven as a particularly versatile tool for the preparation of a wide range of compound semiconductors that would be otherwise difficult or inaccessible by the direct synthesis approaches.[7,8] Most recently, ion exchange reaction was reported for making organic−inorganic perovskites.[9−11] The anion exchange reactions of both $CsPbX_3$ and $CH_3NH_3PbX_3$ (X = I, Br, Cl) perovskite nanocrystals in the solution phase were reported to finely tune optical emission wavelengths.[12−14] Since most of the applications of perovskites are in the form of solid thin films, extending such reactions from the solution phase to the solid phase is of paramount importance for favoring the practical use of this postsynthetic reaction process. Furthermore, the earlier study only demonstrated its role in tuning light emitting properties; its implication in photovoltaics has not been studied so far.

In this work, we demonstrate that the anion exchange reaction of hybrid perovskites can be performed in extended perovskite thin film. More specifically, the anion exchange reaction is processed in the solid phase by a low temperature close space vapor transport process. Despite the reaction being performed in the solid phase, the anion exchange transformation in perovskite thin film is complete and reversible, leading to homogeneous hybrid perovskite film with the morphology conserved and the phase thermodynamically preferred.

2. EXPERIMENTAL SECTION

2.1. Closed Space Vapor Transport and Anion Exchange Reaction. $CH_3NH_3PbI_3$ ($MAPbI_3$) and $CH_3NH_3PbBr_3$ ($MAPbBr_3$) are directly deposited through closed space vapor transport (CSVT) deposition, where precoated PbI_2 and $PbBr_2$ are injected into the CSVT equipment. $MAPbI_3$ and $MAPbBr_3$ are directly formed by the reaction of PbI_2 with the vapor of CH_3NH_3I (MAI) and the reaction of $PbBr_2$ with the vapor of CH_3NH_3Br (MABr), respectively. The anion exchange reaction is accomplished by placing the parent $MAPbI_3$ and $MAPbBr_3$ under the vapor of MABr and MAI, respectively. The process conditions are similar to those used for producing the parent $MAPbX_3$ (X = I, Br). Due to the relatively low pressure and small spacing between the organic halide source and the substrate, the vapor transport is significantly efficient. As a result, the deposition rate is quite fast. The properties of ionic organic salt also ensure that

Received: September 23, 2015
Revised: November 11, 2015
Published: November 13, 2015

DOI: 10.1021/acs.jpcc.5b09300
J. Phys. Chem. C 2015, 119, 26883−26888

the sublimation can be processed at relatively lower temperatures in the form of molecular units as opposed to dissociated ions.

2.2. Perovskite Solar Cell Fabrication. Compact TiO_2 blocking layer was deposited onto the fluorine-doped tin oxide (FTO) coated glass substrate by dc reactive sputtering at 200 °C, followed by spin coating a mesoporous TiO_2 layer composed with 20 nm sized particles using a commercial TiO_2 paste (Dyesol 18 NRT, Dyesol) diluted in ethanol (2:6, weight ratio). The mesoporous TiO_2 layer was annealed at 525 °C for 1 h and then cooled to room temperature. Metal halides were deposited from spin coating PbI_2 (580 mg/mL in dimethylformamide (DMF)) and $PbBr_2$ (440 mg/mL in DMF). The metal halides were then transferred to the CSVT chamber to perform the process. A solution for 2,2′,7,7′-tetrakis(*N*,*N*-di-*p*-methoxyphenylamine)-9,9-spirobifluorene (Spiro-OMeTAD) coating was prepared by dissolving 100 mg of Spiro-OMeTAD (Lumtec) in 1 mL of chlorobenzene, to which 28.8 mL 4-*tert*-butylpyridine and 17.5 mL of a stock solution of 520 mg mL^{-1} lithium bis(trifluoromethylsulfonyl)-imide in acetonitrile were added. Spiro-OMeTAD was deposited at 3500 rpm for 30 s. Finally, 150 nm of silver was thermally evaporated on top of the device to form the counter electrode. The active area of this electrode is 0.1 cm^2.

2.3. Characterization. Current−voltage characteristics were measured using a Keithley 2400 source meter under simulated AM1.5G sunlight at 100 mW cm^{-2} irradiance (Oriel, Sol2A). The light intensity was calibrated by an NREL-calibrated Si reference cell. During the current−voltage measurements, a shadow mask was used to define the cell area. The voltage scan rate was 0.1 V s^{-1}. The *J*−*V* curve was measured with reverse scans, whereas reverse scan defines a measure from the open circuit to the short circuit. X-ray diffraction (XRD) patterns were measured from samples of perovskite deposited on the FTO/TiO_2 (sputtering) substrates using a PANanalytical XRD instrument (model name Empyrean), using Cu Kα radiation (λ = 1.54050 Å). Scanning electron microscopy (SEM) images were obtained using an analytical field emission scanning electron microscope (JSM-7100F, JEOL). The ultraviolet−visible measurement was carried out with normal incidence.

3. RESULTS AND DISCUSSION

3.1. Reversible Anion Exchange Reaction. The anion exchange reaction in the solution phase largely relies on the solvating/ligating environment, the nanocrystal size and shape, and the solubility of outgoing and ingoing ions.[15] The solvating/ligating environment is expected to significantly alter the reduction potential of each cation ion, whereas the nanocrystal size and shape is thought to determine the formation energies for the product and reactant colloid. In the solid-state exchange reaction, there is no need to consider the solvent/ligand or the ion solubility (in solvent). The rigid cationic framework and the anion diffusion ability are the keys to the successful reaction in the solid state.

As expected, for example, in the case of the $MAPbBr_3$, the anion exchange involves replacing the I^- anion in the Pb−CH_3NH_3 framework by Br^-. The Br^- anion enters the Pb−CH_3NH_3 framework as I^- anion diffuses out of the crystal (Figure 1). Surprisingly, when a metal halide film, for example, a PbI_2 film, is placed near the parent $MAPbI_3$ film during the anion exchange process, the PbI_2 film becomes dark brown after the exchange process, although there is a large excess of

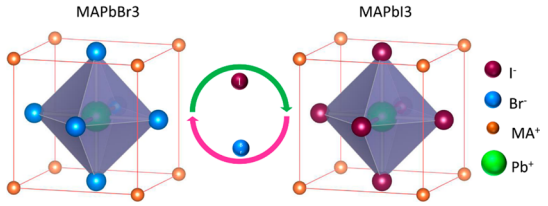

Figure 1. Schematic of the reversible anion exchange reaction within the hybrid halide perovskite. The perovskite is a three-dimensional network formed by an extended framework of corner-sharing PbX_6 octahedra, with $CH_3NH_3^+$ occupying cuboctahedral voids.

MABr vapor around during the MABr sublimation. This observation indicates the out-diffused I^- ion has a higher priority to react with PbI_2 than the Br^- ion in the form of MABr vapor. Therefore, it is expected that the $CH_3NH_3^+$ ion abandoned by Br^- will react with the out-diffused I^- ion, whereas $CH_3NH_3^+$ in the perovskite crystal structure is kept unchanged during the exchange process.

The exchanged $MAPbBr_3$ can be further transformed into $MAPbI_3$ with exposure to the MAI vapor, indicating the anion exchange reaction is reversible (Figure 1). The reversible anion exchange reaction in the perovskite film predicates that the halide ion in it has a high diffusion ability. The high diffusion ability of the halide ion in the perovskite film also ensures easy phase transformation, for example, from tetragonal $MAPbI_3$ to cubic $MAPbBr_3$ and vice versa. This is different from most of the previous anion exchanges in which crystallographic information on the parent crystal, including grain sizes and orientations, is kinetically preserved.[16]

3.2. Crystal Structure, Film Morphology, and Optical Properties. Figure 2 shows the XRD spectra of the film. The direct-deposited $MAPbI_3$ has its main peaks at 13.96, 28.24, and 31.68°, corresponding to a tetragonal crystal structure, while $MAPbBr_3$ shows a set of diffraction peaks of a cubic structured perovskite at 14.78, 21.03, 29.94, and 33.56°. The exchanged $MAPbBr_3$ (or $MAPbI_3$) has the same crystal orientation as the direct-deposited $MAPbBr_3$ (or $MAPbI_3$), suggesting the anion exchange reaction is completed and the phase transformation is thermodynamically preferred as opposed to kinetically controlled. It should be noted that the cubic structure for the $MAPbBr_3$ and the tetragonal structure for the $MAPbI_3$ are thermodynamically stable at the process temperature. The exchanged $MAPbBr_3$ (or $MAPbI_3$) can be transformed into the $MAPbI_3$ (or $MAPbBr_3$) again, along with the expected tetragonal (or cubic) crystal structure.

The phase transformation does not involve large morphology variation, either from $MAPbI_3$ to $MAPbBr_3$ or from $MAPbBr_3$ to $MAPbI_3$, in the forward anion exchange reaction or in the reverse reaction (Figure 3). Although the halide ion diffusion occurs through vacancy-assisted migration instead of the direct exchange of atoms,[17] there is no pore or void formation in the film. The annihilation of the pores or voids in the resulting exchanged film suggests a balancing between the fast outward diffusion and inward diffusion. Otherwise, according to the Kirkendall effect,[18] the deformation of the morphology is unavoidable. The morphology conservation also indicates that the Pb−CH_3NH_3 framework is rigid and the anion displacement manipulations of the halide ions do not seem to affect the cationic sublattice, showing good agreement with the above observation. A recent study using first principles revealed that the activation energy of I^- (0.58 eV) is smaller than that of other species such as Pb_2^+ (2.31 eV) and $CH_3NH_3^+$ (0.84 eV),

DOI: 10.1021/acs.jpcc.5b09300
J. Phys. Chem. C 2015, 119, 26883−26888

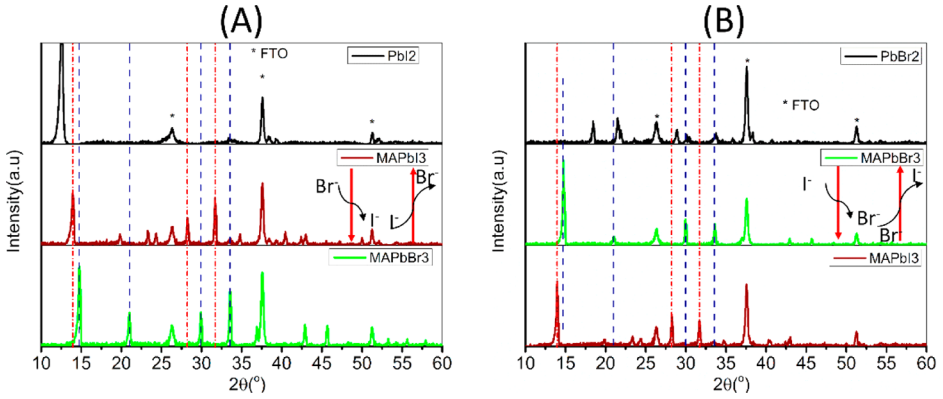

Figure 2. X-ray diffraction (XRD) patterns of the metal halides (PbI_2 and $PbBr_2$), parent $MAPbX_3$ (X = I, Br), and anion exchanged samples, showing the transformation of phase from cubic perovskite structure ($MAPbBr_3$) to tetragonal perovskite structure ($MAPbI_3$), and vice versa.

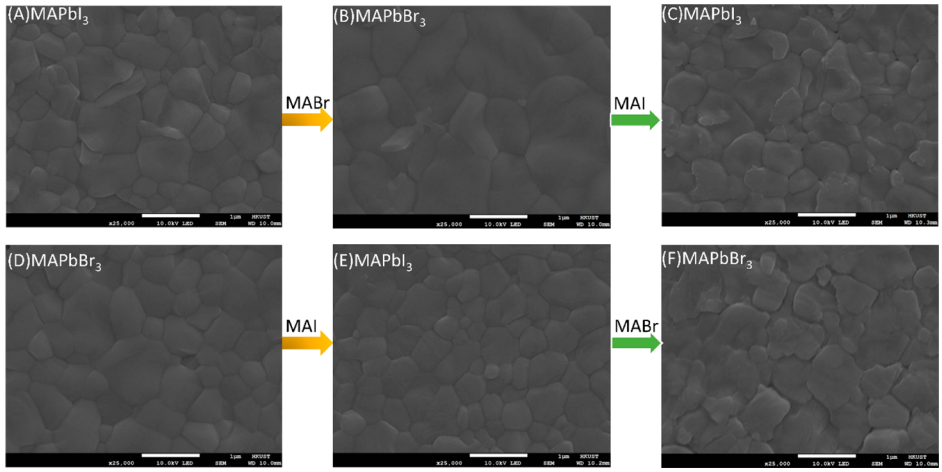

Figure 3. SEM images of perovskite films. (A, D) Parent perovskites ($MAPbI_3$ and $MAPbBr_3$) directly fabricated from the metal halides and organic halides in a typical CSVT process; (B, E) perovskites fabricated from anion exchange reactions; (C, F) perovskites fabricated from the reverse anion exchange reactions.

further confirming the robust nature of the Pb−CH_3NH_3 framework and the high diffusion ability of the halide in the perovskite network.[17] In turn, the easy halide exchange reaction explains the ionic transport behavior in hybrid perovskites. However, with the reverse anion exchange reaction, the surface becomes much rougher. Long-time exposure of the sample to the vapor may be responsible.

The absorption spectra are measured to characterize the optical band gaps of the perovskite obtained from direct deposition and anion exchange reaction (Figure 4). Both the direct-deposited and anion exchanged perovskites have almost the same absorption behavior for $MAPbI_3$ and $MAPbBr_3$, respectively. This similar absorption behavior suggests that the anion exchange reaction does not induce any remarkable in-gap defect states that would lead to deterioration of the optical properties. The optical band gap is also not changed, as demonstrated by the good consistency of the sharp band edge in both cases. By extrapolating the distinct linear region of the absorption edge to the abscissa in the Tauc plot, we determine the optical band gaps of $MAPbI_3$ and $MAPbBr_3$ to be 1.59 and 2.29 eV, corresponding to the featured wavelengths of 780 and 540 nm, respectively. In the case of $MAPbBr_3$, there is a peak near the band gap in the absorption spectrum, which is often attributed to an excitonic transition. This excitonic transition

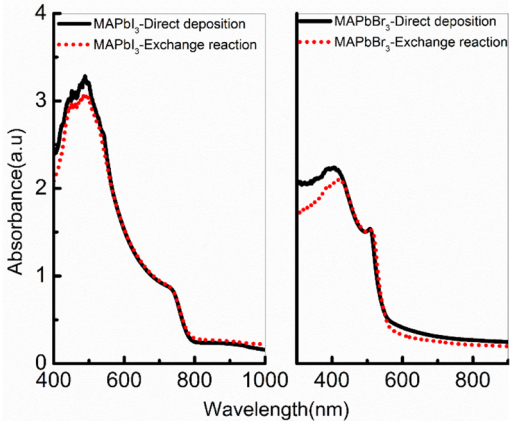

Figure 4. Absorbance spectra of $MAPbI_3$ and $MAPbBr_3$ fabricated from either direct deposition or anion exchange reaction.

was also observed in the large-grain and single crystal $MAPbBr_3$.[19]

3.3. Application in Perovskite Solar Cells. In order to investigate the influence of the anion exchange process on the material quality, solar cells with different $MAPbBr_3$ and $MAPbI_3$ absorbing layers are fabricated. Figure 5A shows the schematic of the energy band diagram of the cells. The cell is

DOI: 10.1021/acs.jpcc.5b09300
J. Phys. Chem. C 2015, 119, 26883−26888

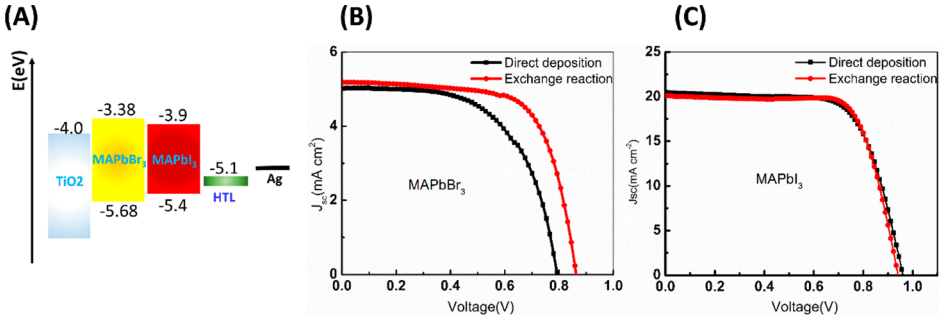

Figure 5. (A) Schematic energy diagram of $MAPbBr_3$ and $MAPbI_3$ solar cells; (B) current−voltage curve of solar cells with $MAPbBr_3$ fabricated from direct deposition and anion exchange reaction; (C) current−voltage curve of solar cells with $MAPbI_3$ fabricated from direct deposition and anion exchange reaction.

constructed on fluorine-doped tin oxide (FTO) coated glass. A compact layer of sputtering TiO_2 and a mesoporous TiO_2 are used as the n-type layers. Perovskites deposited from either the direct deposition or anion exchange reaction are used as the absorbers. The p-type hole conductor, 2,2′,7,7′-tetrakis(*N*,*N*-di-*p*-methoxyphenylamine)-9,9-spirobifluorene (Spiro-OMeTAD), and a Ag contact are then deposited to finish the cell process.

Table 1 shows the performance of the solar cells with $MAPbBr_3$ and $MAPbI_3$ fabricated through direct deposition and anion exchange reaction. Figure 5B,C shows the corresponding *J*−*V* curves. Although $MAPbBr_3$ has a larger energy band gap than $MAPbI_3$, the cell obtained from the direct reaction of MABr and $PbBr_2$ does not show the larger V_{oc} that may be expected from its larger band gap. With the anion exchange process, in which the $MAPbBr_3$ layer is fabricated from the exchanged parent $MAPbI_3$, there is a slight increase of the V_{oc} as well as the J_{sc}, indicating that the anion exchange does not induce any remarkable defects resulting from the lattice transformation and morphology reconstruction. In the direct deposition and anion exchange reaction $MAPbI_3$ cells have the same trend as that of the $MAPbBr_3$ cells. In perovskite solar cells, hysteresis is widely observed between current−voltage measurements performed at different scan rates and directions.[20,21] The hystereses of $MAPbBr_3$ and $MAPbI_3$ cells fabricated from the anion exchanged reaction are investigated by changing the scan rates and directions. As shown in Figure S1, there is little hysteresis observed in the $MAPbBr_3$ cells, whereas significant hysteresis is found in the $MAPbI_3$ cells. The reason for the different hysteresis behaviors in the $MAPbBr_3$ and $MAPbI_3$ cells is still not clear to us at present.

Table 1. Characteristics of $MAPbBr_3$ and $MAPbI_3$ Solar Cells Obtained from Direct Deposition and Anion Exchange Reaction[a]

top cell (structure)	V_{oc} (V)	FF[b] (%)	J_{sc} (mA/cm^2)	PCE (%)
$MAPbBr_3$				
direct deposition	0.8	55	5.0	2.2
exchange reaction	0.86	68	5.2	3.0
$MAPbI_3$				
direct deposition	0.96	70	20.5	13.8
exchange reaction	0.94	74	20.2	14.0

[a]Values are obtained from an average of four cells for each. [b]Fill factor.

A special case is that when the PbI_2 is used in fabrication of $MAPbBr_{3-x}I_x$, a remarkable improvement of the device performance is obtained (Figure S2). Particularly, V_{oc} is improved from 0.8 V ($PbBr_2$ as the precursor) to 1.3 V (PbI_2

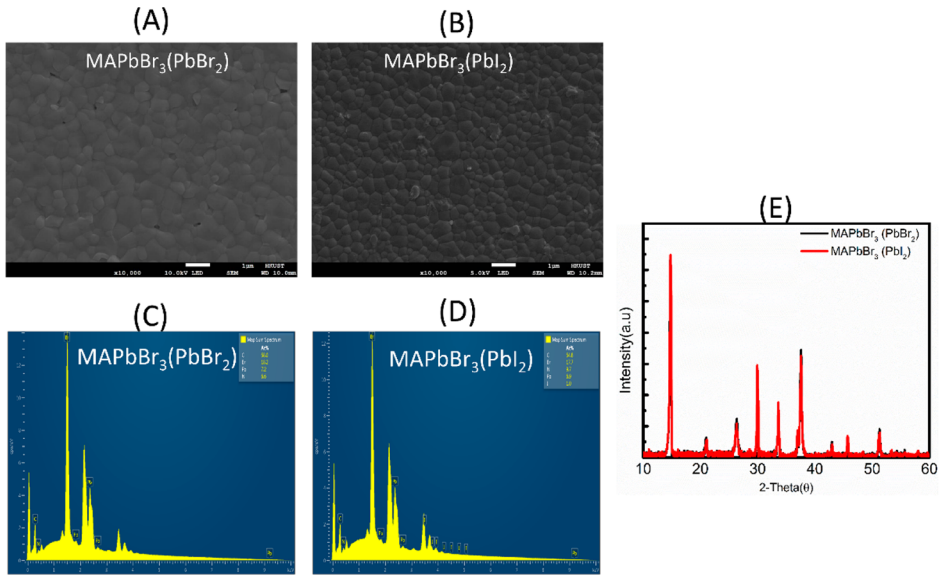

Figure 6. (A, B) Film morphology, (C, D) energy-dispersive X-ray spectroscopy, and (E) XRD of $MAPbBr_3$ fabricated from either PbI_2 or $PbBr_2$.

DOI: 10.1021/acs.jpcc.5b09300
J. Phys. Chem. C 2015, 119, 26883−26888

as the precursor). However, these two perovskites have no significant difference in crystal structure, film morphology, and composition (Figure 6). It is worth noting that Spiro-OMeTAD has its highest occupied molecular orbital (HOMO) at 5.1 eV and TiO_2 has its lowest unoccupied molecular orbital (LUMO) at 4.0 eV (Figure 5A). The energy difference between the HOMO and LUMO is therefore only 1.1 eV, and the 1.3 V V_{oc} obtained suggests that $MAPbBr_3$ acts as the absorbing layer as well as the p-type layer. However, the FF is poor probably due to interface defects resulting from the large energy level difference between the E_v of $MAPbBr_3$ (−5.68 eV) and the HOMO of the hole transport layer (HTL) (−5.1 eV).[22] Better FF and V_{oc} can be further expected by using some HTLs with lower HOMO. Indeed, in the reaction of PbI_2 with MABr, the iodine in the metal halide is mostly removed from film and displaced by Br (Figure 6D). Because the I^- in the form of PbI_2 cannot experience the exchange reaction, excess Br^- will only react with the PbI_2 to form an intermediate state, and then the I^- ion in the intermediate state will be displaced by Br^-. The simultaneous displacement reaction and crystallization involves the beneficial exchange of halide species, and together with the high diffusion ability of the halide ion, high quality perovskite can be obtained. However, when we further applied this to $MAPbI_3$ by adopting $PbBr_2$ as the precursor, there is no difference in the solar cell performance. Further explanation is required to understand such a difference.

4. CONCLUSIONS

In summary, we have demonstrated the anion exchange reaction in extended solid perovskite thin film by converting the iodine-based to the bromine-based formulation. Although the reaction is performed in the solid phase, it is remarkably fast, complete, and reversible, which is clearly evidenced from the XRD, SEM, and optical measurements. The obtained exchanged perovskite compound is homogeneous, morphology conserved, and phase thermodynamically preferred, suggesting the robust nature of the $Pb-CH_3NH_3$ framework and high diffusion ability of halide ions in the perovskite lattice. These findings are helpful to understanding the perovskite formation mechanism and the ionic behavior in the perovskite. Furthermore, the good consistency of the optical absorbance in directly deposited and anion-exchanged perovskite indicates that the anion exchange reaction does not induce any remarkable in-gap defect states that would lead to deterioration of the optical properties, which is also confirmed by the solar cell results. Finally, in some cases, we show that the simultaneous displacement reaction and crystallization process may be beneficial to use to improve the material quality.

■ ASSOCIATED CONTENT

Supporting Information

The Supporting Information is available free of charge on the ACS Publications website at DOI: 10.1021/acs.jpcc.5b09300.

Hysteresis behavior, device performance of $MAPbBr_3$ solar cells fabricated with PbI_2 and $PbBr_2$ (PDF)

■ AUTHOR INFORMATION

Corresponding Authors

*Tel.:+852 23588845. E-mail: gliad@connect.ust.hk (G.L.).
*Tel.:+852 23587056. E-mail: eekwok@ust.hk (H.S.K.).

Notes

The authors declare no competing financial interest.

■ ACKNOWLEDGMENTS

This work was funded by the Partner State Key Laboratory on Advanced Displays and Optoelectronics Technologies (PSKL) through Project No. ITC-PskL12EG02. The work was partially supported by a grant from the Research Grants Council of the Hong Kong Special Administrative Region, China, under Theme-based Research Scheme through Project No. T23-713/11-1.

■ REFERENCES

(1) Yang, W. S.; Noh, J. H.; Jeon, N. J.; Kim, Y. C.; Ryu, S.; Seo, J.; Seok, S. I. High-Performance Photovoltaic Perovskite Layers Fabricated through Intramolecular Exchange. *Science* **2015**, *348* (6240), 1234−1237.

(2) Stranks, S. D.; Eperon, G. E.; Grancini, G.; Menelaou, C.; Alcocer, M. J. P.; Leijtens, T.; Herz, L. M.; Petrozza, A.; Snaith, H. J. Electron-Hole Diffusion Lengths Exceeding 1 Micrometer in an Organometal Trihalide Perovskite Absorber. *Science* **2013**, *342* (6156), 341−344.

(3) Liu, M.; Johnston, M. B.; Snaith, H. J. Efficient Planar Heterojunction Perovskite Solar Cells by Vapour Deposition. *Nature* **2013**, *501* (7467), 395−398.

(4) Xing, G.; Mathews, N.; Sun, S.; Lim, S. S.; Lam, Y. M.; Gratzel, M.; Mhaisalkar, S.; Sum, T. C. Long-Range Balanced Electron- and Hole-Transport Lengths in Organic-Inorganic CH3NH3PbI3. *Science* **2013**, *342* (6156), 344−347.

(5) Green, M. A.; Ho-Baillie, A.; Snaith, H. J. The Emergence of Perovskite Solar Cells. *Nat. Photonics* **2014**, *8* (7), 506−514.

(6) Li, G.; Ching, K. L.; Ho, J. Y. L.; Wong, M.; Kwok, H.-S. Identifying the Optimum Morphology in High-Performance Perovskite Solar Cells. *Adv. Energy Mater.* **2015**, DOI: 10.1002/aenm.201401775.

(7) Gupta, S.; Kershaw, S. V.; Rogach, A. L. 25th Anniversary Article: Ion Exchange in Colloidal Nanocrystals. *Adv. Mater.* **2013**, *25* (48), 6923−6944.

(8) Rivest, J. B.; Jain, P. K. Cation Exchange on the Nanoscale: An Emerging Technique for New Material Synthesis, Device Fabrication, and Chemical Sensing. *Chem. Soc. Rev.* **2013**, *42* (1), 89−96.

(9) Solis-Ibarra, D.; Smith, I. C.; Karunadasa, H. I. Post-Synthetic Halide Conversion and Selective Halogen Capture in Hybrid Perovskites. *Chem. Sci.* **2015**, *6* (7), 4054−4059.

(10) Pellet, N.; Teuscher, J.; Maier, J.; Grätzel, M. Transforming Hybrid Organic Inorganic Perovskites by Rapid Halide Exchange. *Chem. Mater.* **2015**, *27* (6), 2181−2188.

(11) Wong, A. B.; Lai, M.; Eaton, S. W.; Yu, Y.; Lin, E.; Dou, L.; Fu, A.; Yang, P. Growth and Anion Exchange Conversion of CH3NH3PbX3 Nanorod Arrays for Light-Emitting Diodes. *Nano Lett.* **2015**, *15* (8), 5519−5524.

(12) Akkerman, Q. A.; D'Innocenzo, V.; Accornero, S.; Scarpellini, A.; Petrozza, A.; Prato, M.; Manna, L. Tuning the Optical Properties of Cesium Lead Halide Perovskite Nanocrystals by Anion Exchange Reactions. *J. Am. Chem. Soc.* **2015**, *137* (32), 10276−10281.

(13) Jang, D. M.; Park, K.; Kim, D. H.; Park, J.; Shojaei, F.; Kang, H. S.; Ahn, J.-P.; Lee, J. W.; Song, J. K. Reversible Halide Exchange Reaction of Organometal Trihalide Perovskite Colloidal Nanocrystals for Full-Range Band Gap Tuning. *Nano Lett.* **2015**, *15* (8), 5191−5199.

(14) Nedelcu, G.; Protesescu, L.; Yakunin, S.; Bodnarchuk, M. I.; Grotevent, M. J.; Kovalenko, M. V. Fast Anion-Exchange in Highly Luminescent Nanocrystals of Cesium Lead Halide Perovskites ($CsPbX_3$, X = Cl, Br, I). *Nano Lett.* **2015**, *15* (8), 5635−5640.

(15) Beberwyck, B. J.; Surendranath, Y.; Alivisatos, A. P. Cation Exchange: A Versatile Tool for Nanomaterials Synthesis. *J. Phys. Chem. C* **2013**, *117* (39), 19759−19770.

DOI: 10.1021/acs.jpcc.5b09300
J. Phys. Chem. C 2015, 119, 26883−26888

(16) Dloczik, L.; Koenenkamp, R. Nanostructured Metal Sulfide Surfaces by Ion Exchange Processes. *J. Solid State Electrochem.* **2004**, *8* (3), 142−146.
(17) Eames, C.; Frost, J. M.; Barnes, P. R. F.; O'Regan, B. C.; Walsh, A.; Islam, M. S. Ionic Transport in Hybrid Lead Iodide Perovskite Solar Cells. *Nat. Commun.* **2015**, *6*, 7497.
(18) Nakajima, H. The Discovery and Acceptance of the Kirkendall Effect: The Result of a Short Research Career. *JOM* **1997**, *49* (6), 15−19.
(19) Yang, Y.; Yan, Y.; Yang, M.; Choi, S.; Zhu, K.; Luther, J. M.; Beard, M. C. Low Surface Recombination Velocity in Solution-Grown CH3NH3PbBr3 Perovskite Single Crystal. *Nat. Commun.* **2015**, *6*, 7961.
(20) Unger, E. L.; Hoke, E. T.; Bailie, C. D.; Nguyen, W. H.; Bowring, A. R.; Heumüller, T.; Christoforo, M. G.; McGehee, M. D. Hysteresis and Transient Behavior in Current−voltage Measurements of Hybrid-Perovskite Absorber Solar Cells. *Energy Environ. Sci.* **2014**, *7* (11), 3690−3698.
(21) Tress, W.; Marinova, N.; Moehl, T.; Zakeeruddin, S. M.; Nazeeruddin, M. K.; Grätzel, M. Understanding the Rate-Dependent J−V Hysteresis, Slow Time Component, and Aging in $CH_3NH_3PbI_3$ Perovskite Solar Cells: The Role of a Compensated Electric Field. *Energy Environ. Sci.* **2015**, *8* (3), 995−1004.
(22) Seo, J.; Park, S.; Chan Kim, Y.; Jeon, N. J.; Noh, J. H.; Yoon, S. C.; Seok, S. I. Benefits of Very Thin PCBM and LiF Layers for Solution-Processed P−i−n Perovskite Solar Cells. *Energy Environ. Sci.* **2014**, *7* (8), 2642.

DOI: 10.1021/acs.jpcc.5b09300
J. Phys. Chem. C 2015, 119, 26883−26888